

Contents lists available at ScienceDirect

Cement and Concrete Composites

journal homepage: www.elsevier.com/locate/cemconcomp





Carbon capture and storage potential of biochar-enriched cementitious systems

Geetika Mishra^a, Panagiotis A. Danoglidis^b, Surendra P. Shah^c, Maria S. Konsta-Gdoutos^{c,*}

- a Center for Advanced Construction Materials, The University of Texas at Arlington, 701 S Nedderman Dr., Arlington, TX, 76019, USA
- b Center for Advanced Construction Materials, Department of Civil Engineering, The University of Texas at Arlington, 701 S Nedderman Dr, Arlington, TX, 76019, USA
- ^c Center for Advanced Construction Materials, Civil Engineering, The University of Texas at Arlington, 701 S Nedderman Dr, Arlington, TX, 76019, USA

ARTICLE INFO

Keywords: Biochar CO_2 sequestration Mineralization Fly ash Crack propagation

ABSTRACT

A promising solution to nullify the net embodied greenhouse gas emissions of civil infrastructure is the use of carbon-negative materials for concrete manufacturing. Carbon-neutral coal ash and agriculture/forestry byproducts, such as biochar, exhibit a high carbon dioxide (CO₂) uptake potential. The aim of the study is to explore the viability of using biochar as a carbon sink and to develop carbon-neutral concrete with improved performance. Experimental findings suggest that the optimal amount of biochar (1%) slightly improves hydration and mechanical properties, but the combination with mineral additives significantly enhances the performance. Thermogravimetric analysis (TGA) revealed that compared to OPC, the addition of 1% biochar contributes to a 42% increase in CO₂ uptake, while the combination of biochar with 10% class C fly ash further increases CO₂ capture capacity of the mix by 92%. Under accelerated carbonation conditions, the biochar-enriched mortars exhibit a 20% higher modulus of elasticity indicating an effectively increased stiffness over the reference carbonated OPC. The carbonated biochar mortars also exhibit up to 64% increased toughness indices indicating the material's great resistance to crack coalescence and propagation at the strain softening stage. Scanning Electron Microscopy and Energy Dispersive X-ray Spectroscopy (SEM-EDS) results validated our prediction that the porous morphology of biochar promoted enhanced CO₂ absorption and in-situ mineralization of calcium carbonate, resulting in a denser and stronger cement matrix.

1. Introduction

Increased carbon dioxide (CO_2) emission is becoming a serious threat to the environment, wherein cement is one of the top commodities contributing about 7% of anthropogenic CO_2 emissions globally, mainly due to rapid urbanization. Adopting alternative materials in the construction sector to sequester or capture atmospheric CO_2 and utilize it in the development of value-added building components can help address these sustainability issues. Biochar is a porous byproduct of the biomass pyrolysis process, which involves the thermochemical conversion of biomass at temperatures between 450 and 550 $^{\circ}C$ in the absence of oxygen [1,2]. Biochar is considered a carbon-negative material, as carbon is locked in its structure during preparation. It has the potential to offset 12% of anthropogenic CO_2 emissions by 2050, with estimated sequestration of 0.3–2 Gt CO_2 per year [3]. Properties of biochar depend on several factors such as type of feedstock, preparation parameters, and

by-product usage [4]. Biochar has been intensively investigated as a material for soil amendment, water, and air filtration due to its unique porosity and water retention ability [5]. As a carbon-sequestering mineral additive for cement-based materials, biochar is currently attracting interest in academia and industry [6-10]. If biochar can replace a fraction of cement in a targeted concrete that will perform as well as plain concrete, it would be a win-win alternative for lowering CO₂ emissions and at the same time developing environment-friendly carbon-neutral concrete [11]. So far studies have reported that in biochar-cementitious composites the increase in hydration products observed has the potential of creating more carbonate mineralization sites in the cementitious matrix [12]. Some contradicting results have been reported about the effect of biochar on cement hydration. While Wang et al. [13] noticed greater heat of hydration after 48 h of curing in mixtures with 2% biochar indicating a small increase in overall hydration, other researchers found no effects on cement hydration when using

E-mail addresses: geetika.mishra@uta.edu (G. Mishra), panagiotis.danoglidis@uta.edu (P.A. Danoglidis), surendra.shah@uta.edu (S.P. Shah), maria.konsta@uta.edu (M.S. Konsta-Gdoutos).

^{*} Corresponding author.

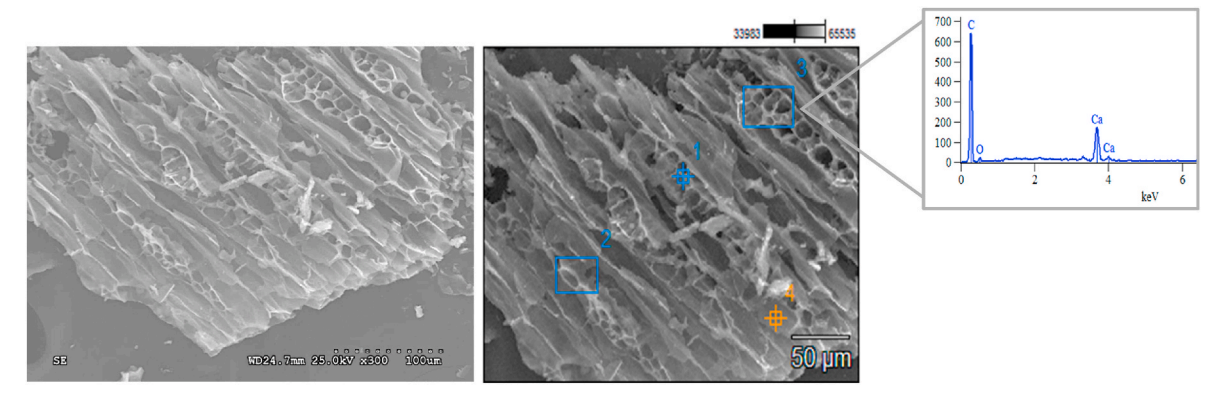


Fig. 1. SEM-EDS micrographs of biochar.

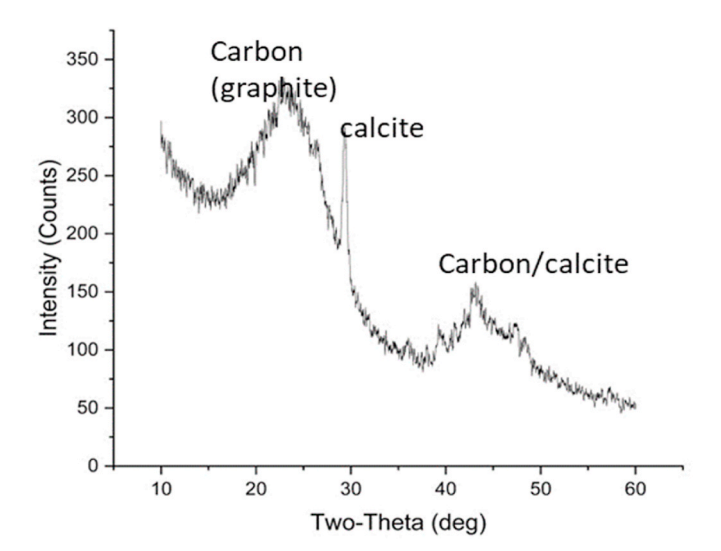


Fig. 2. XRD profile of "as received" biochar.

biochar at amounts up to 5% [14]. Biochar's significant carbon content was found to have an interesting effect on the mechanical and fracture characteristics of the biochar cementitious mixes. Restuccia et al. [15] and Ahmad et al. [16] found that the pyrolyzed biochar micro-particles, which are characterized by high strength and stiffness due to their significant carbon content, increase the crack tortuosity, hence promoting the toughening mechanism of the cementitious matrix. As a result, the fracture energy values of biochar enriched cementitious composites are about 40% higher compared to OPC [17].

Little information is available on combining biochar with mineral admixtures and their effects on the diffusivity of CO2 and carbonate mineralization. Gupta et al. [18] investigated the effect of biochar on silica fume mixes and concluded that silica fume, due to its pozzolanic activity, can offset the reduced strength observed in biochar mortars. The pozzolanic activity of the additives mainly varies with the change in composition, particle size, and morphologies. In a recent study by Akhtar et al. [19], rapid carbonation caused by the addition of biochar to fly ash blocks resulted in more CO2 absorption. Similarly, Gupta et al. [20] observed that biochar-fly ash composites sequestered 7%-13% CO2, while reducing water absorption and chemical shrinkage on carbonation. Drying shrinkage however increased by 39%, owing to the presence of impurities in the biochar. It should be noted here that while pozzolanic materials/mineral additives are important resources for increasing economically the viability of concrete and improving strength and durability, the diffusivity of CO2 and the carbonate mineralization process in a cementitious matrix enriched with pozzolans are profoundly influenced, mainly due to the reduction of calcium hydroxide (CH), which may result in 20–60% reduction in concrete's carbon sequestration potential [21–23]. However, the impact of carbonation was mostly examined in pozzolan enriched cements as a durability attribute; the effect on ${\rm CO_2}$ uptake capacity has not been thoroughly investigated.

Given the demonstrated CO_2 sequestration potential of biochar, it is envisioned that in a mix with biochar, fly ash and/or nanosilica, the biochar's highly porous nature will greatly affect the diffusion kinetics and uptake of CO_2 ; hence a higher rate of carbonate mineralization may potentially be observed. To the best of the authors' knowledge, no prior research has examined the CO_2 storage capability of concrete, enriched with pozzolanic and biochar components and its effect on fracture properties. Therefore, the objective of this study is to systematically examine the physical and chemical interactions between biochar, fly ash and/or nanosilica in cementitious mortars, and the enormous prospect of CO_2 uptake and in situ mineralization process, in an effort to providing scientific insights into this novel and cleaner approach. Class C fly ash was chosen for the CO_2 mineralization pathway due to its high calcium content [24].

2. Experimental work

2.1. Materials

In this study, paste and mortar specimens were fabricated using Type I ordinary Portland cement (OPC) 42.5 R and standard sand according to ASTM C 778-17 [25]. Class C fly ash confirming with ASTM C 618 [26] and powdered nano silica (NANOSHEL, USA) were used to study the synergistic effect with biochar. Biochar was obtained from a local vendor, and it contained more than 90% carbon with bulk density of 0.55 g/cm³. Scanning electron microscopy (SEM) was used to identify the morphology of the biochar particles. Imaging was conducted at the potential of 25 kV after coating the biochar specimens with platinum sputter coater. Energy Dispersive X-ray Spectroscopy (EDS) was also used for the elemental mapping of biochar. Particle size of biochar varies between 20 and 250 µm with irregular shapes (shown in Fig. 1), which could serve as interlocking agents. Additionally, they have a porous microstructure with surface micropores that range in size from 5 to 10 μm. These pores generally form due to the emission of volatiles and organic matter during pyrolysis, which can absorb water and act as a self-curing agent in mortar and concrete [27]. The semi-amorphous crystal structure of biochar together with the presence of calcite at 29.3 (2θ) was shown in Fig. 2, using X-ray diffraction. To quantitatively evaluate the amount of calcite in "as received" biochar and class C fly ash, thermogravimetric analysis (TGA) was performed. The TGA results for "as received" biochar and class C fly ash are presented in Figs. 3 and 4, respectively. The amount of calcite was calculated from the weight loss in the temperature range of 500–900 $^{\circ}$ C. It was found that the "as received" biochar and fly ash contain 44% and 0.54% of calcite,

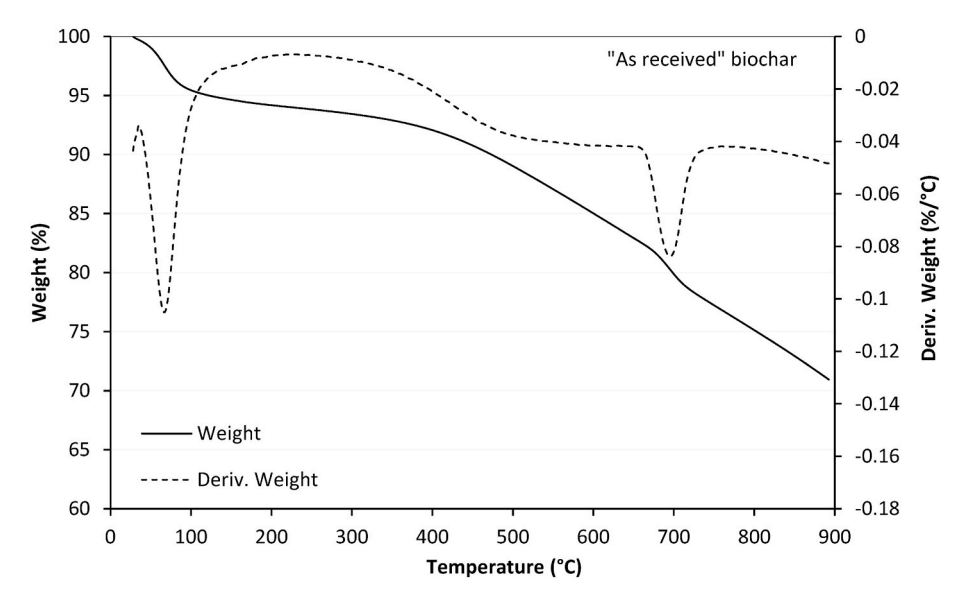


Fig. 3. TGA curve of "as received" biochar.

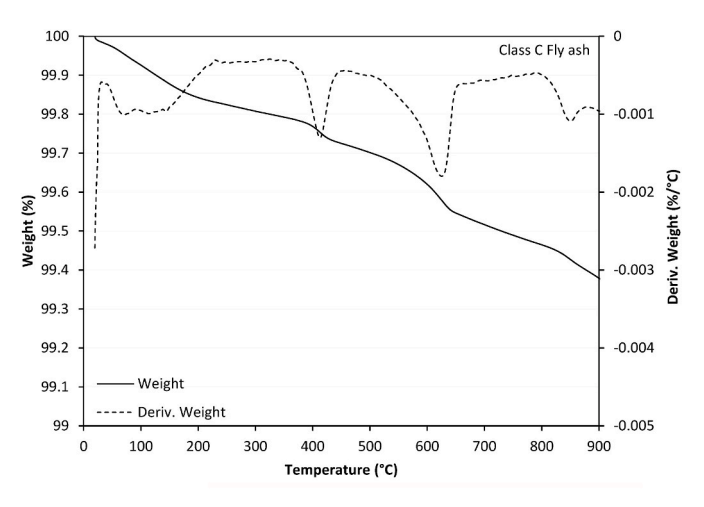


Fig. 4. TGA curve of Class C Fly ash.

Table 1
Mix compositions.

	Mix	Cement (g)	Biochar (g)	Fly ash (g)	Nanosilica (g)
1	Cement mortar (CM)	960	_		-
2	CM + B1	950.4	9.6	-	_
3	CM + B1.5	945.6	14	-	_
4	CM + B1+C-FA10	854.4	9.6	96	_
5	CM + B1 + NS1	940.8	9.6	-	9.6

respectively.

2.2. Sample preparation

Five different combinations were investigated in the present study and the mix proportions are shown in Table 1. The water-to-cement and sand-to-cement ratios were kept at 0.485 and 2.75, respectively for all mixes. Biochar at amounts of 1% and 1.5 wt% was added to replace cement. Combinations of biochar-fly ash and biochar-nano silica were also investigated, where 10 wt% fly ash and 1 wt% nano-silica were combined with 1 wt% biochar. Carboxylate-based superplasticizer was

used to maintain the workability of all the mortar mixes same as plain cement mortar. A standard Hobart mixer capable of operating from 140 to 285 rpm was employed. According to the mixing procedure the cement, biochar, and fly ash or nano-silica were placed in the mixing bowl and mixed for 30 s at a speed of 140 rpm. The entire quantity of sand was then added over a 30 s period while mixing at the speed of 140 rpm. Finally, water was added to the mortar mixture and mixed for 90 s at a speed of 285 rpm. The mixture was cast in $4 \times 4 \times 16$ cm³ molds for the three-point bending tests. Following demolding (at 24 h), the samples were cured in a moist chamber at controlled temperature and humidity of 23 °C and 95%, respectively till the time of testing. After 3 days of moist curing, a few samples were moved to a carbonation chamber with the set condition of 12% CO₂ (100% purity) supplied at 15 psi, 23 \pm 5 °C and 65 \pm 3% relative humidity for 7 days, which corresponds to 10 days from the time of casting, to assess carbon capture capacity. The exposure concentration of CO2 was selected to mimic the thermal power plant emission and to ensure the suitability of biochar for carbon capture in an accelerated environment.

2.3. Testing methods

An isothermal conduction calorimeter was used to measure the heat of hydration of freshly mixed paste samples. Samples were mixed with distilled water in a plastic ampoule at a speed of $200 \pm 10 \text{ r/min}$ for 180 s, in accordance with the ASTM C1679 [28]. Thermogravimetric analysis (TGA) experiments following the ASTM C1872 [29] were conducted on 7- and 28- day specimens to determine the chemically bound water and the amount of calcium hydroxide (CH) and calcium carbonate (CaCO₃). For TGA, approximately 50 mg of the paste was cored and wet-ground with isopropanol to stop the hydration [30]. The weight loss was monitored throughout the temperature range of 20–900 °C at a ramp of 15 °C/min, with the fixed flow of nitrogen 50 ml/min as purge gas during the heating process. The weight loss occurring during the decomposition of hydrated cement across the temperature range (105–900 °C) was considered for quantifying combined/bound water (W_c) using Eq. (1) [31].

$$W_c = W_{(h)} + W_{CH} + 0.41(W_{CC})$$
 (1)

Where $W_{(h)}$, W_{CH} , and W_{CC} are the loss of water due to dehydration of C–S–H/C-A-S-H, ettringite etc (105–400 °C), de-hydroxylation of CH (400–500 °C) and decarbonation (550–900 °C) respectively. The conversion factor for the mass loss due to CaCO₃ to the molecular weight of

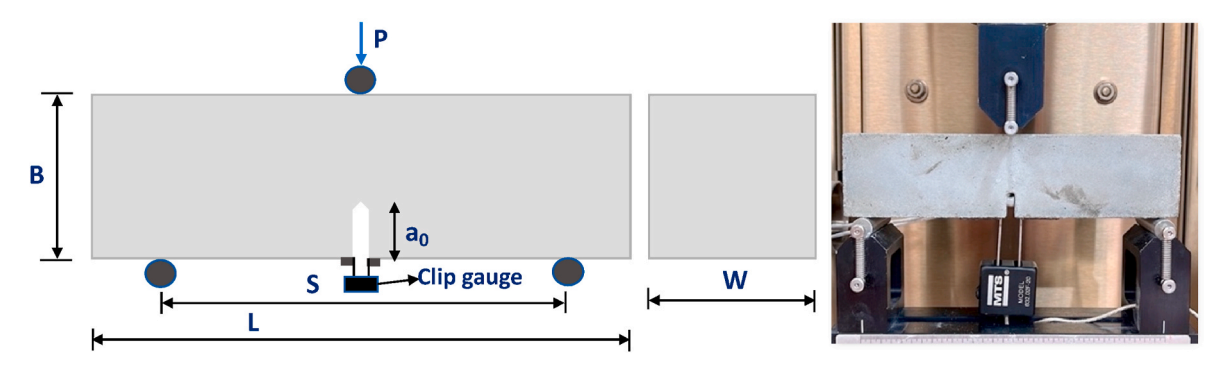


Fig. 5. Experimental setup for the 3-point bending.

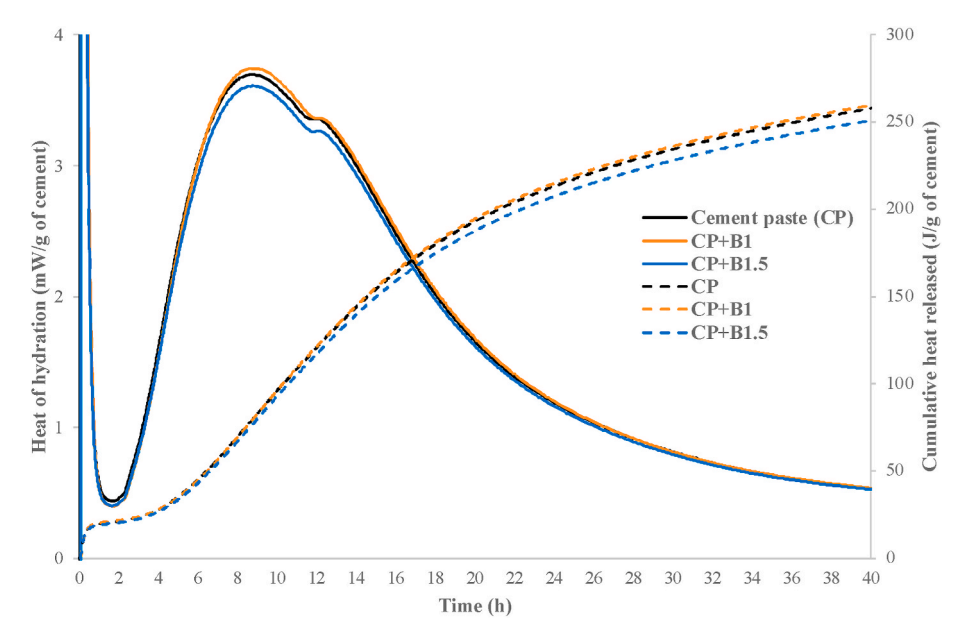


Fig. 6. Heat of hydration (solid lines) and cumulative heat released (dashed lines) curves of biochar-cement pastes.

water in CH is 0.41 in Eq. (1). CH, $CaCO_3$, and CO_2 uptake were calculated using equations (2)–(4) [20,32].

$$CH(\%) = \frac{M_{400} - M_{500}}{M_{\odot}} \times 4.1 \times 100 \tag{2}$$

$$CaCO_3(\%) = \frac{M_{525} - M_{900}}{M_c} \times 2.27 \times 100$$
 (3)

$$CO_2 \ uptake \ (\%) = \left(\frac{M_{525} - M_{900}}{M_c}\right) \times 100$$
 (4)

Where M_{400} , M_{500} , M_{525} , and M_{900} represent the sample masses (g) at their respective ignition temperatures and M_c is the mass of anhydrous cement heating to 1000 °C and corrected for the loss of ignition of cement, biochar and Class C fly ash used in the study. The molecular weight ratios of Ca(OH)₂ to H₂O, and CaCO₃ to CO₂ are 4.1 and 2.27, respectively.

Three-point bending tests were conducted to assess the flexural strength and Young's modulus of non-carbonated and carbonated mortars following the Linear Elastic Fracture Mechanics (LEFM) [33,34]. Notched $4\times4\times16~{\rm cm}^3$ specimens were prepared and tested in three-point bending at the age of 3, 7 and 28 days (Fig. 5). The prismatic specimens were cut using a water-cooled band saw with a 13.3 mm notch and the length of the notch was determined as per the RILEM, which requires a notch-to-depth ratio of 1/3 [35]. As the feedback signal, a crack mouth opening displacement (CMOD) extensometer was

employed to create steady crack propagation at a rate of 0.001 mm/min. The strain softening behavior, which expresses the material's resistance to crack propagation when the micro- and macro-cracks coalesce to form a fracture zone at the post-peak region, was also assessed by evaluating the size-independent toughness indices, $\rm I_5$ and $\rm I_{10}$, from the load-CMOD curves following the RILEM TC 162 [36].

The three-point bending specimens were broken into two halves, and the resulting prisms were tested for compressive strength and Young's modulus using ASTM C349-20 [37] and ASTM C109/109 M-20, respectively [38]. After the three-point bending test, the halves were inspected for any cracks that may have formed before the uniaxial compression test. For the testing, a 500 kN MTS servo-hydraulic, closed-loop equipment with displacement control was used. A constant velocity of 0.3 mm/s was maintained.

3. Results and discussions

3.1. Effect of biochar on cement hydration

The reactivity of biochar depends on the type of biomass from which it is derived. Results about the effect of biochar on the rate of cement hydration are conflicting, reporting occasional acceleration of the hydration rate [13,14]. The isothermal calorimetry results in Fig. 6 present the effect of biochar addition on cement hydration. The curve shows that compared to plain OPC paste the addition of 1 wt% biochar to cement paste marginally increases the heat of hydration; while increasing

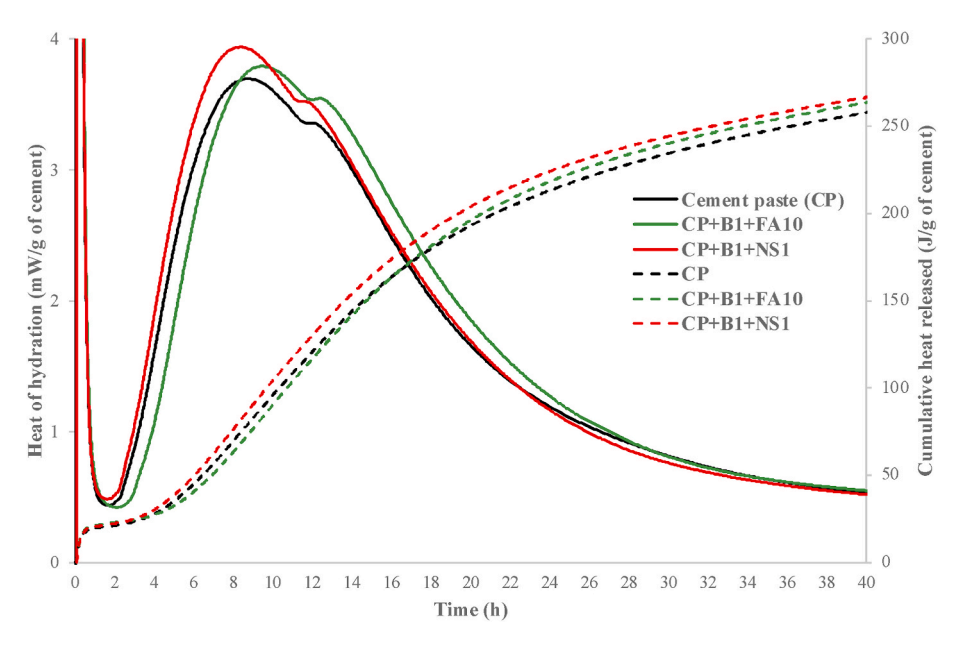


Fig. 7. Heat of hydration (solid lines) and cumulative heat (dashed lines) released curve of biochar-fly ash and biochar-nanosilica cement pastes.

Table 2Chemically bound water of non-carbonated cement paste calculated from TGA.

	Chemically bound water (%)		
	7 days	28 days	
СР	17.89	20.91	
CP + B1	17.77	20.87	
CP + B1.5	17.40	21.01	
CP + B1 + C-FA10	16.83	21.97	
CP + B1 + NS1	18.96	22.99	

further the amount of biochar to 1.5 wt% slightly reduces the heat of hydration, probably due to the insulating effect of the carbon in the biochar structure. Poppe et al. [39] have also observed that adding high inert filler content reduces heat development during the hardening stage of cement. Comparing the cumulative heat released during hydration also confirmed that the amount of 1 wt% biochar could be safely utilized in OPC mixtures owing to a similar hydration behavior to that of plain cement. It is also observed from Fig. 6 that increasing the replacement level of cement with biochar i.e., 1.5 wt% marginally reduces the cumulative heat released.

The effect of fly ash and nano-silica on the hydration of the biochar cementitious mixes was also evaluated. From Fig. 7, one can observe that using the optimal amount of biochar (1 wt%), in combination with 10 wt% fly ash and 1 wt% nano-silica, compared to reference samples (without biochar) at 40 h of hydration increases the hydration heat by 2.3% and 5.6%, respectively. As expected, the addition of nano-silica to the biochar-cement mix, compared to OPC, accelerates the cement hydration and significantly increases the heat released. This is attributed to the synergistic effect of nano silica and biochar, wherein nano-silica acts as a nucleating site for faster dissolution of cement phases, and biochar helps in moisture regulation during the hydration process [40,41]. This conclusion agrees with previous findings suggesting that biochar retains moisture in its porous structure and regulates the hydration of cement with the progress of time [42]. However, in our study, it was noticed that the incorporation of only biochar does not accelerate or delay the cement hydration kinetics; hence biochar could be used as a green additive in concrete. It is also observed from Fig. 7 that the addition of 10 wt% fly ash delayed the hydration reaction in the first 12 h. Due to the slow reactivity of fly ash particles, dissolution-precipitation process slows down at early hydration age and causes an extended dormant period with respect to plain OPC. However, with the progress of hydration time, the cumulative heat released in the FA-biochar mix (CP + B1+FA10) eventually reached a level comparable to the nanosilica-biochar mix (CP + B1+NS1), owing to the pozzolanic reaction of fly ash after crystallization of calcium hydroxide. This observation revealed that the use of fly ash and nano-silica in the biochar-OPC mix contributes to improving the hydration mechanism. This implies that the introduction of additional supplementary cementitious material with biochar might further open the avenue for saving more cement.

Furthermore, to observe the effect of biochar with mineral additives on the formation of hydration products in 7 and 28 days, chemically bound water was calculated. Table 2 presents the bound water for OPCbiochar pastes at 1% and 1.5 wt% replacement levels, and with the combination of fly ash and nano-silica. The addition of biochar marginally reduces the bound water, probably due to replacing a small fraction of cement with an inert filler, producing relatively fewer hydration products. As mentioned earlier adding an optimum amount of biochar does not accelerate or delay the hydration, thus no remarkable change should be observed in the amount of bound water. A similar trend was observed with the addition of fly ash at early hydration age (7 days). The results showed that a reduction of 11% of cement led to a decrease in hydration products, which subsequently led to a 5.9% reduction in bound water. On the other hand, the addition of nano-silica resulted in a significant increase in bound water, as its high surface area provided additional surface for the precipitation of hydration products.

After 28 days, the amount of chemically bound water of the OPC-biochar mix increased with hydration time and attained comparable quantities to the control sample. The mechanism behind this is not well understood. A hypothesis put forward suggests an internal curing mechanism contributed by biochar releasing moisture from its microstructure and leading to an increased cement hydration process [43]. Moreover, in the fly ash-biochar cement mix, compared to the plain OPC, bound water increased subsequently by 5.0% indicating the formation of additional hydration products due to pozzolanic reaction at later age. Similarly, the amount of chemically bound water of the nanosilica-biochar cement mix (CP + B1+NS1) significantly increased over time due to the superior pozzolanic activity of the nanosilica.

From the discussion above it is evident that in the fly ash and nanosilica biochar-cementitious mix, the mesoporous structure of biochar provides sites for the deposition of the additional hydrates formed due to the pozzolanic reaction and rapid nucleation. This process of

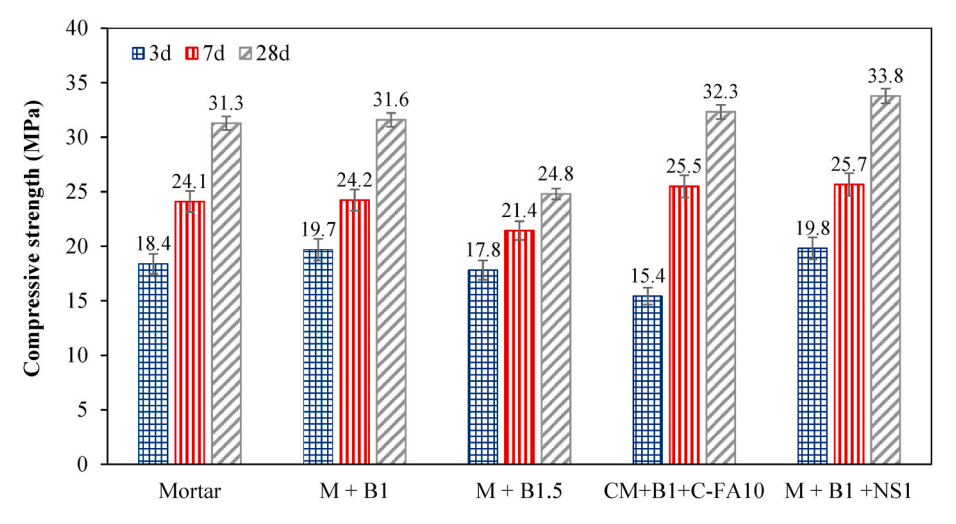


Fig. 8. Compressive strength of non-carbonated samples.

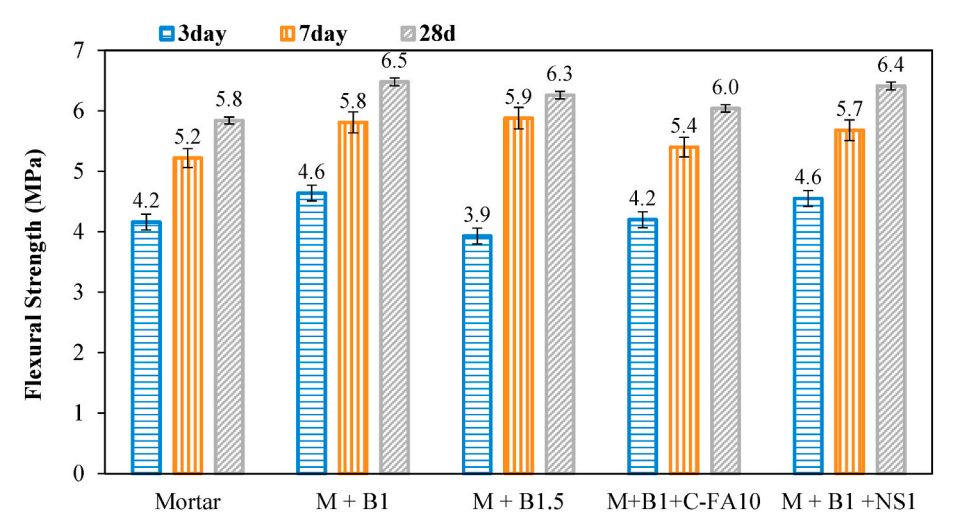


Fig. 9. Flexural strength of non-carbonated samples.

rapid cement phase dissolution and hydrate precipitation reduces the inter-particle empty spaces (or inter-connected capillary pores) and contributes to a more uniform distribution of the hydration products. Consequently, the combination of biochar and mineral additives has a synergistic effect in enhancing the hydration mechanism.

3.2. Effect of biochar on the strength of OPC, fly-ash and nanosilica mortars

The average compressive strength of OPC, fly ash, and nanosilicamortars modified with biochar at 3, 7 and 28 days is shown in Fig. 8. The addition of biochar at an amount of 1 wt% slightly increases the compressive strength of OPC mortars as it is shown by the 5–7.5% higher strength values. As explained earlier, biochar does not exhibit any hydraulic property, therefore, this enhancement at an early age may be the result of a filler effect and the fine particle size of the biochar. Increasing the biochar dosage to 1.5 wt% results in negligible increases of the early age compressive strength, while with increased hydration time a lower by 26% compressive strength is observed at 28 days. The results are in accordance with the literature suggesting that the addition of biochar concentrations higher than 1 wt% reduces the compressive strength of OPC mixes, due to the mesoporous structure of biochar [44]. Moreover, compared to OPC and OPC-biochar mortars, the combination of 1% biochar with 10% fly ash results in a slightly improved compressive

strength at the 7- and 28- day probably due to the different particle sizes and shapes of the fly ash and biochar particle, which can offer improved binary packing in the cementitious matrix that enhances strength. Alongside, fly ash serves as an effective pozzolanic material enabling the conversion of CH to C-S-H, which is the primary hydration product responsible for the strength development of the cementitious materials. It is also worth mentioning here that the performance of the biochar-fly ash mix was not compromised even after replacing 11 wt% of cement with fly ash and biochar. This result highlights the great potential of carbon-negative waste by-products such as biochar and fly ash contributing to the manufacturing of carbon-neutral concrete. In contrast to the biochar-fly ash mortar, the combination of biochar and nano-silica results in 7–9% higher compressive strength compared to the OPC and OPC-biochar mortars. This is attributed to the refined microstructure of the cement matrix by filling inter-particle spaces with additional hydration products, as shown in the SEM micrographs in Fig. 10. Previous studies also revealed that the combined use of biochar-fly ash significantly enhances the bond strength and cohesiveness of solid particles hence increasing the physicomechanical properties of the composites [45]. Enhanced pore filling by hydration products would lead to improvement in mechanical strength through the densification of the cementitious matrix [46].

The flexural strength values of the cement mortars modified using biochar, fly ash, and nano-silica at the age of 3, 7 and 28 days are

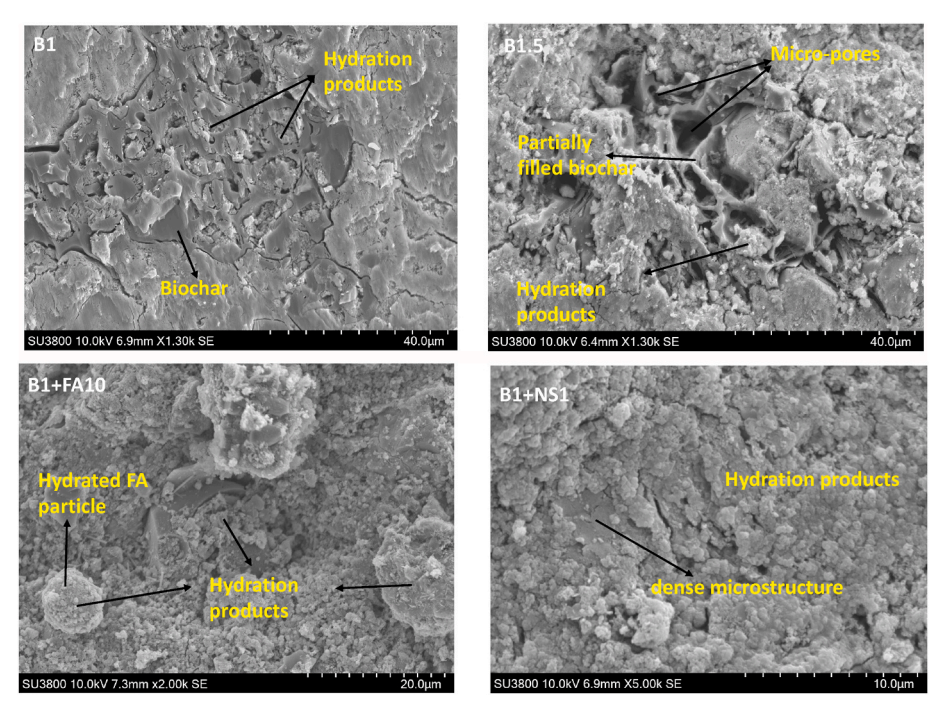


Fig. 10. SEM micrographs of non-carbonated biochar-enriched cement pastes (B1 and B1.5) combined with fly ash (B1+FA10) and nanosilica (B1+NS1).

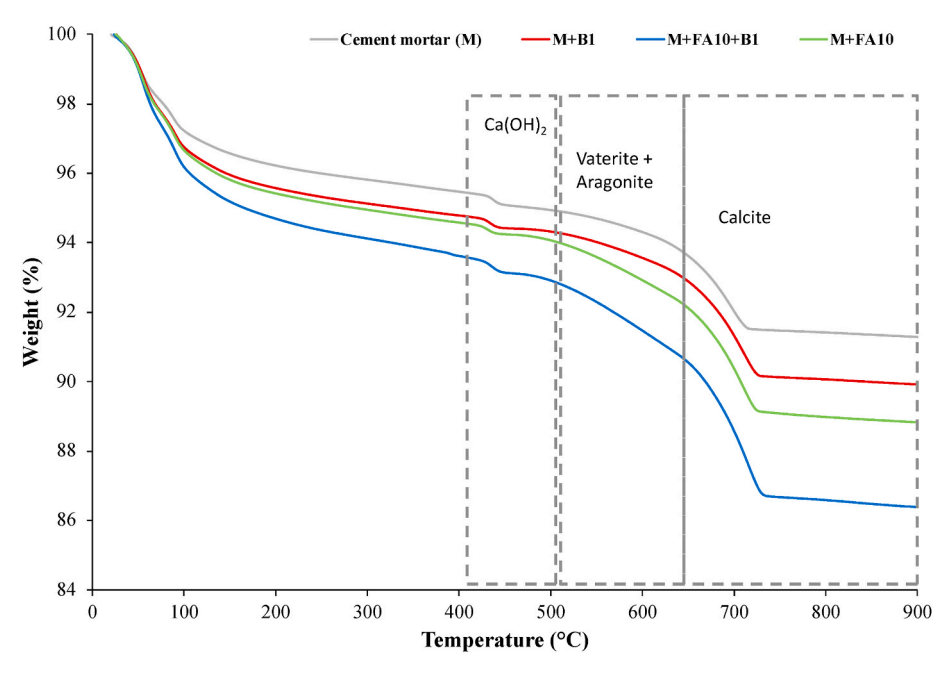


Fig. 11. TGA curve of biochar and fly ash added biochar mortar after 7 days of carbonation.

Table 3TGA analysis of 7-day carbonated specimens.

Mix	Sample	CH (%)	CaCO ₃ (%)	CO ₂ uptake (%)
1	Cement mortar (CM)	1.78	8.72	3.84
2	CM + B1	1.55	12.41	5.46
3	CM + FA10	1.66	13.88	6.11
4	CM + FA10+B1	1.42	16.78	7.39

presented in Fig. 9. The addition of 1% and 1.5 wt% biochar increases the flexural strength by 11.5% and 13.4% at 7 d, and 12% and 8.6% at 28 d compared to plain mortar. This is attributed to the improved

interface with the biochar particles filled with hydration products. Results from the SEM micrographs of the specimens' fractured surfaces, shown in Fig. 10, revealed carbon-inert microparticles that act as obstacles in the crack growth path and deflect around the biochar microstructure filled with hydration products. The inclusion of fly ash or/and nanosilica further densified the microstructure and enhanced the flexural strength compared to the OPC-biochar samples.

3.3. Effect of biochar on carbon capture capacity

The carbon capture capacity of mortars with B1, FA10, and a combination of fly ash and biochar (FA10+B1) was investigated. We chose

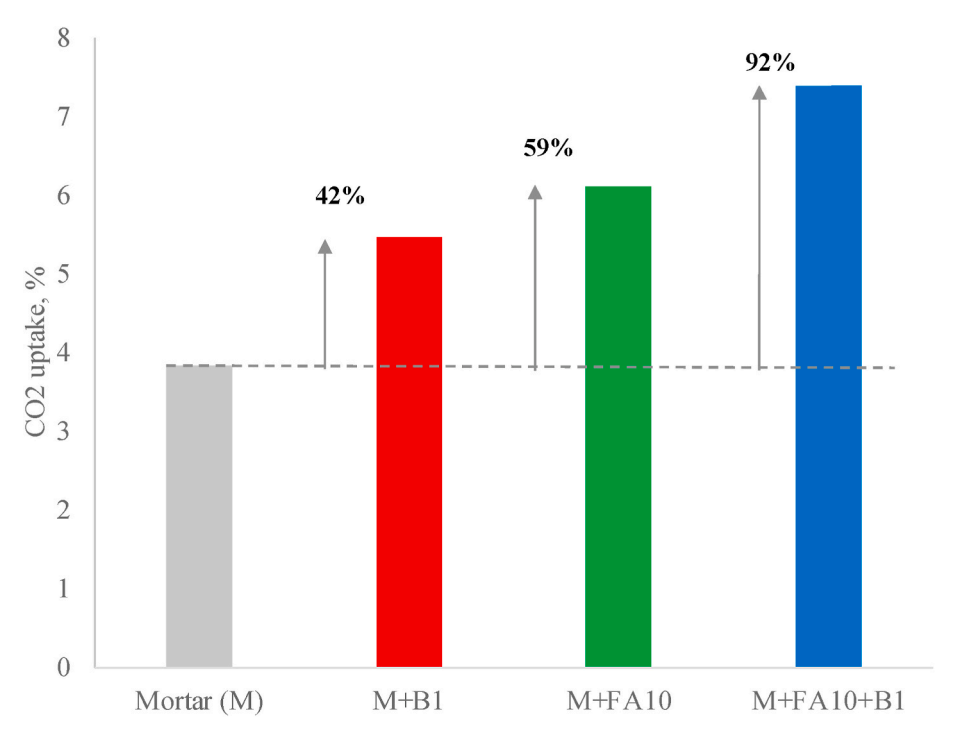


Fig. 12. Increase in CO2 uptake after 7 days of carbonation.

Table 4Mechanical properties of 7-day carbonated specimens.

	Flexural Strength (MPa)	Compressive Strength (MPa)
OPC Mortar (M)	5.39 ± 0.55	25.81 ± 1.89
M + B1	5.77 ± 0.43	25.97 ± 1.84
M + FA10	5.59 ± 0.41	25.14 ± 1.02
$M+FA10{+}B1$	5.80 ± 0.43	26.03 ± 1.83

to use class C fly ash because of its high calcium content, which could help in the reaction with diffused CO_2 and the subsequent mineralization process. As demonstrated earlier, the presence of nano-silica resulted in the development of a refined and denser microstructure due to nucleation and pozzolanic reaction starting from a very early age of hydration, which could potentially limit the pathways for the diffusion of CO_2 in the cementitious matrix. Therefore, in this section, the

potential for CO_2 capture and mineralization in concrete will be studied using an optimal amount of biochar (1 wt%), only in combination with fly ash.

The CO_2 uptake potential of the OPC-biochar mix was evaluated using TGA on specimens kept in CO_2 chamber for 7 days, after 3 days of normal curing. CO_2 curing of cementitious materials is a diffusion-controlled reaction that depends on several factors such as the concentration of CO_2 , time of exposure, and moisture gradient [47,48]. A previous study observed that increasing the water-cement ratio from 0.25 to 0.45 resulted in a constant rise in CO_2 sequestration from 40 g CO_2 /kg to 175 g CO_2 /kg of clinker at a CO_2 concentration of 50%. Higher CO_2 diffusion into the cementitious matrix is attributed to increased porosity due to the availability of a sufficient amount of moisture for the dissolution of CO_2 [49]. Therefore, this study was carried out on specimens prepared with w/c = 0.485, kept under accelerated carbonation conditions. Bertos et al. [50] reported that the

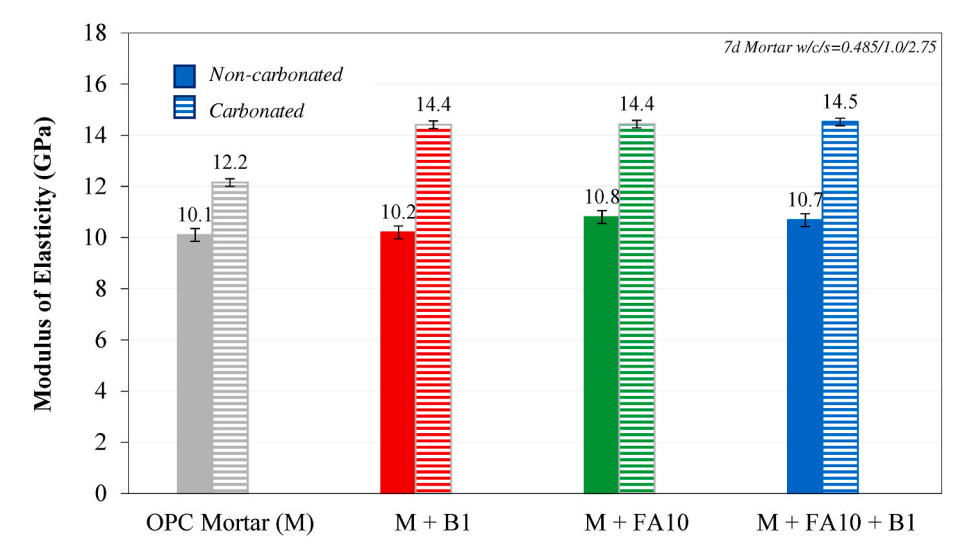


Fig. 13. Modulus of Elasticity of 7-day non-carbonated and carbonated OPC and OPC-fly ash mortars modified with 1% biochar.

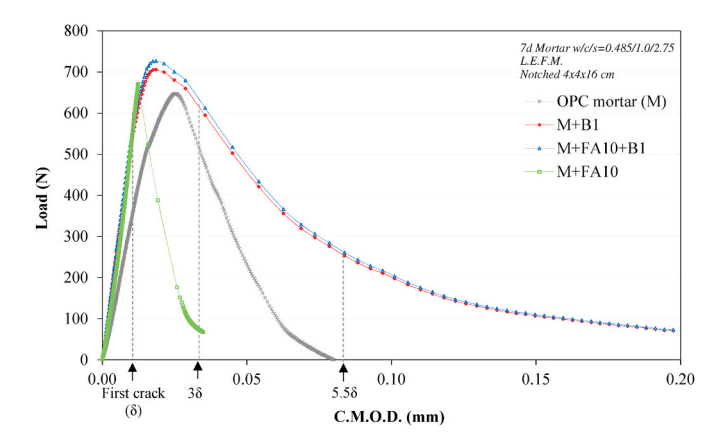


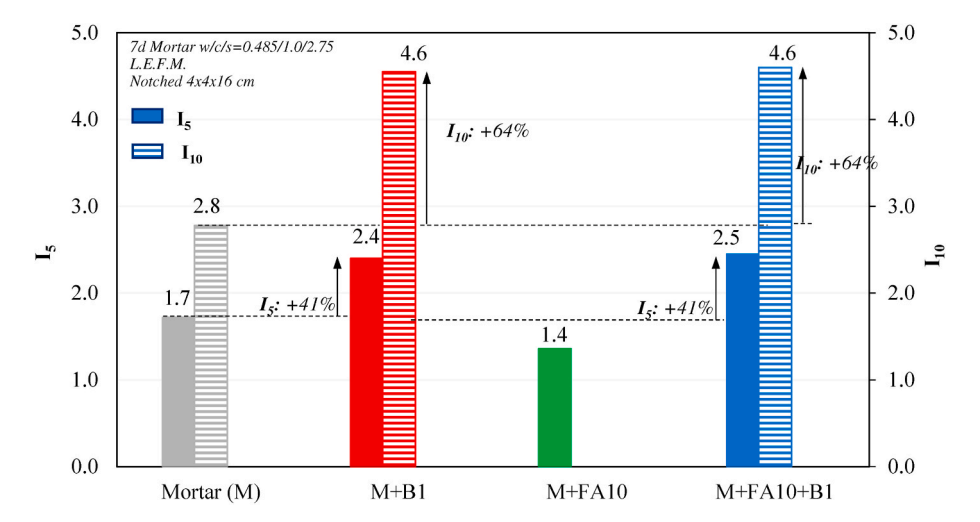
Fig. 14. Load-CMOD curves of mortars with biochar and fly ash after 7 days of carbonation.

continued exposure of specimens to CO_2 for a long time may affect results due to the generation of a dense membrane of carbonates around the interior anhydrous cement and hydration products, hindering further CO_2 diffusion and reaction. Thus, due to the supply of high CO_2 concentration (12%) at high pressure of 1 bar, the ingress of CO_2 is recorded at early hydration age, in this study. The mass change curve of carbonated biochar and the combination of biochar with fly ash obtained from TGA can be seen in Fig. 11, where the mass loss in the range 400 °C–500 °C represents the dehydration of CH and 530 °C–900 °C, considered for the decomposition of different polymorphs of calcite. From the TGA curve, it can be seen that the addition of biochar and fly ash (M + FA10+B1), compared to the other mixes, results in lower

amounts of CH and increased amounts of calcite due to mineralization. It is speculated that the availability of the porous pathways provided by the biochar facilitated the diffusion of $CO_{2,}$ and the abundance of free Ca^{2+} ions from the class C fly ash accelerated the precipitation of carbonates. To validate this mechanism, a quantitative analysis of $CaCO_{3}$ and CH was conducted and provided in Table 3.

Table 3 illustrates the calculation of the amount of $CaCO_3$ in mixes with biochar, fly ash, and the combination of biochar-fly ash. The amount of total calcium carbonate including three polymorphs aragonite, vaterite, and calcite is calculated based on the weight loss in the temperature range of 530–900 °C due to the decarbonization of all polymorphs of calcium carbonates. The decarbonation of calcium carbonate in the range of 530–650 °C corresponds to the decomposition of poorly crystalline carbonates (i.e vaterite and aragonite), and in the range of 650–1000 °C to the decomposition of well crystalline calcite [51].

Compared to plain OPC (8.72%), the amount of calcium carbonate was observed 12.41%, 13.88%, and 16.78% in biochar, fly ash, and combined biochar-fly ash mixes, respectively. The increase in carbonate mineralization in the biochar mix (B1) is attributed to the mesoporous volume and pore area of biochar, which expedited the ingress of $\rm CO_2$ in the cement matrix; while in fly ash mixes (FA10), carbon mineralization was significantly higher due to the rapid dissolution of calcium ions from fly ash during $\rm CO_2$ curing. Accelerated carbon curing enhanced the hydration activity and resulted in higher precipitation of $\rm CaCO_3$ which should also lead to an improved strength [52]. Moreover, when FA10 and B1 are combined in the CM + FA10+B1 mix, the synergistic effect of fly ash and biochar further enhanced the formation of carbonates. Interestingly, it is observed that the $\rm CO_2$ uptake capacity of the biochar-fly ash mix is 7.3%, which translates to a 92% increase (shown



 $\textbf{Fig. 15.} \ \ \text{Toughness indices I}_{5} \ \text{and I}_{10} \ \text{of 7 d carbonated mortars with fly ash and/or biochar.}$

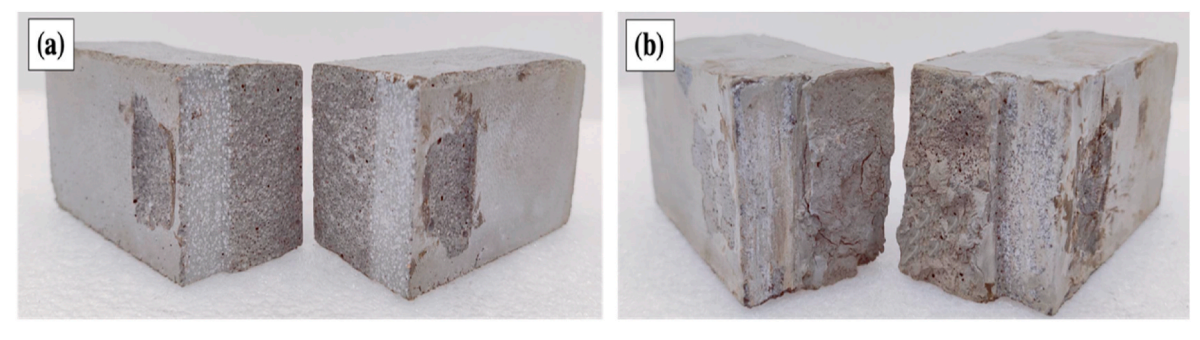


Fig. 16. Typical fracture surfaces of the carbonated cement composites tested in flexure (a) Plain mortar (b) biochar-enriched cement mortar.

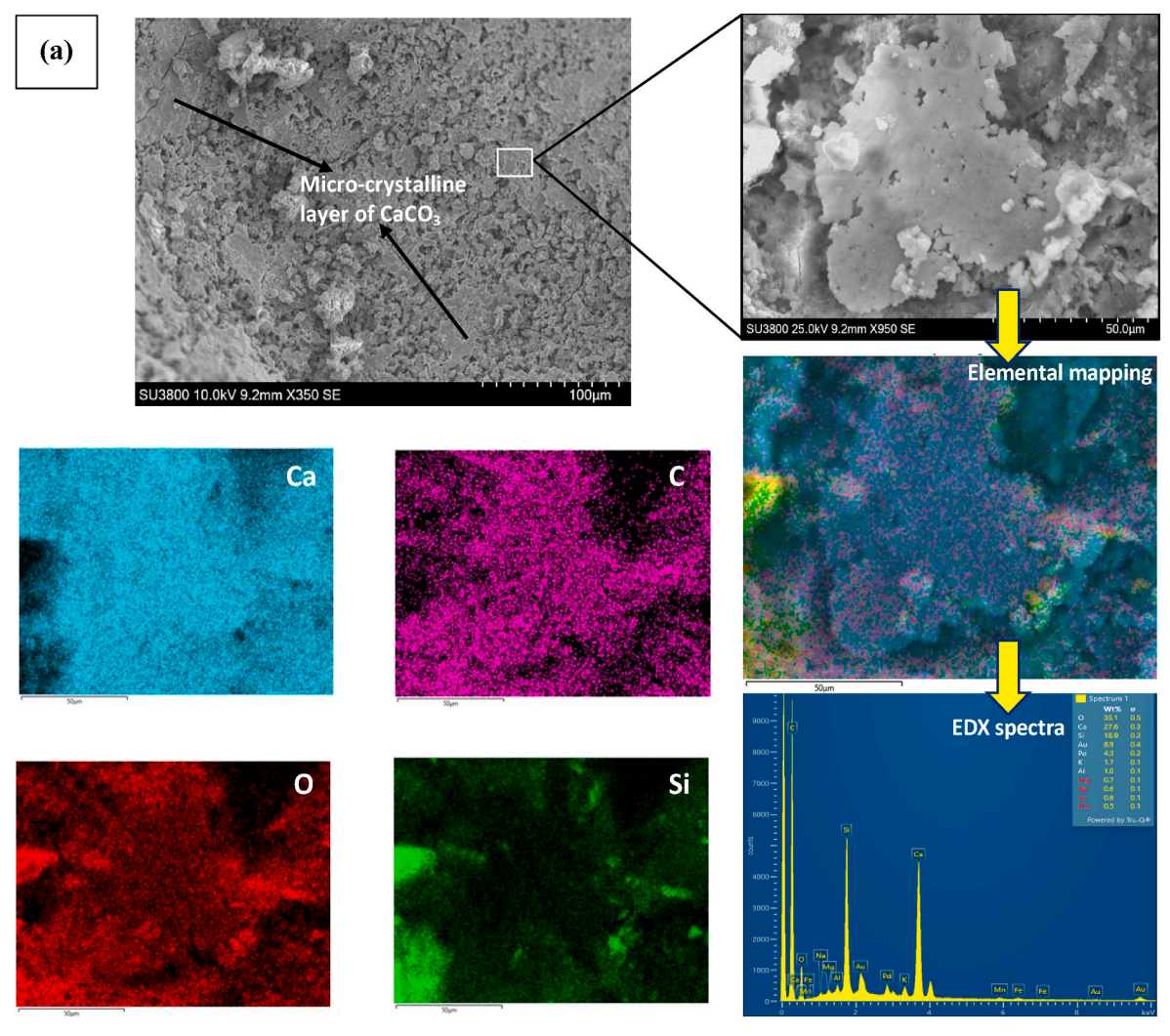


Fig. 17. SEM images and EDS elemental mapping of (a) carbonated OPC, and (b and c) carbonated biochar enriched OPC-fly ash mortar.

in Fig. 12) when compared with the CM + B1 (42%) and CM + FA10 (59%). It should be noted that the concentrations of calcite included in the 1 wt% pristine "as received" biochar (0.44%) and 10% class C fly ash (0.054%), defined by the TGA analysis of the pristine materials in Figs. 3 and 4 respectively, were subtracted from the calculations of CaCO $_3$ (%) and CO $_2$ uptake (%) in 7-day carbonated specimens in Table 3.

The reduction of CH content is obvious in all the mixes due to carbonation and transformation into $CaCO_3$. This finding implies that combining biochar with high calcium pozzolan is a novel approach for sequestering CO_2 and permanently storing the formed mineral within the cementitious matrix. The research into the use of biochar in concrete production is still in its early stages, and additional research is needed to fully comprehend its potential and economic viability.

3.4. Effect of biochar on the strength, stiffness and crack propagation resistance of carbonated biochar – OPC and fly ash mortars

The compressive and flexural strength results of the 7-day carbonated plain cement, fly ash, and biochar-enriched OPC and fly ash mortar are presented in Table 4. It is observed that under accelerated carbon curing, the biochar cement mortar exhibits 3–10% higher compressive and flexural strength compared to the samples without the biochar addition. This is attributed to the higher CaCO $_3$ content in biochar-enriched mortars, than the plain OPC and fly ash mortars, as revealed by the TGA analysis results in Table 3. The modulus of elasticity of non-

carbonated and carbonated 7-day OPC and fly ash mortars with 1 wt% biochar is presented in Fig. 13. All the non-carbonated samples exhibit almost the same modulus of elasticity ranging from 10.1 GPa to 10.8 GPa. On the other hand, the carbonated biochar and/or fly ash cementitious mortars exhibit 20% higher modulus of elasticity indicating an effectively increased stiffness over the reference carbonated OPC. This is attributed to the precipitation of higher ${\rm CaCO_3}$ content in biochar OPC and fly ash mortars during carbonation which increases the volume of the solid phase due to pore filling and crack healing, which leads to the densification of the matrix [53]. Therefore, higher amounts of elastic energy can be absorbed by the densified matrix, improving the carbonated material's elastic behavior [54].

Load-CMOD curves of the 7-day carbonated mortar and fly ashmortar specimens with 1 wt% biochar addition are presented in Fig. 14. The load-CMOD curves of plain and modified mortars exhibit similar patterns with a linear elastic stage before peak load and a nonlinear stage of stable crack propagation up to failure. It is observed however that the load-CMOD ratio at the linear elastic stage and the peak load of biochar-enriched fly ash mortars are higher than the OPC mortar, leading to the observed increases in modulus of elasticity (Fig. 13). The carbonated fly ash-mortar exhibits a brittle behavior as it is indicated by the reduced post-peak load-CMOD stage (CMOD at failure \approx 0.03 mm) compared to the reference carbonated mortar (CMOD at failure \approx 0.08 mm). The brittle behavior of carbonated fly-ash concrete has been reported previously in the literature [55]. On the other hand,

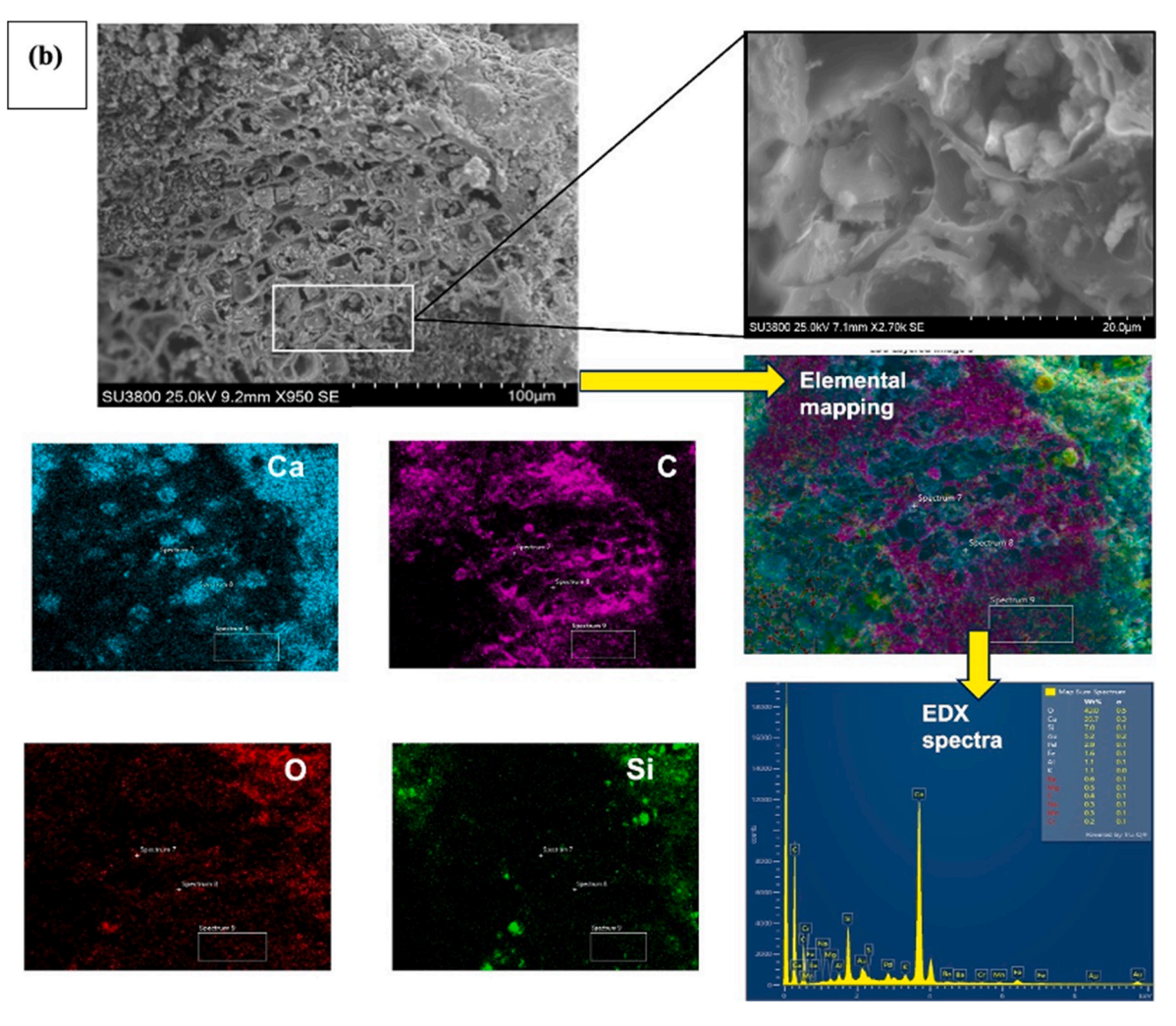


Fig. 17. (continued).

the carbonated biochar-cementitious specimens exhibit markedly elongated load-CMOD curves with 150% higher CMOD values at failure ($\approx\!0.20$ mm) compared to the reference ($\approx\!0.08$ mm) and fly ash-mortar ($\approx\!0.03$ mm). The results indicate a remarkably increased post-peak energy absorption capability, thus, improved strain-softening behavior, despite the high CaCO $_3$ content (Table 3) that has the potential to increase the embrittlement of concrete and fly ash-concrete [56, 57]

To quantitatively evaluate the carbonated materials' energy absorption capability at the post-cracking area the dimensionless toughness indices I_5 and I_{10} were calculated by dividing the area up to a CMOD of 3.0 and 5.5 times the CMOD at first-crack (δ) by the area up to first crack, as it is shown in Fig. 15 [58]. The carbonated mortars exhibit 30% lower toughness indices I_5 and I_{10} compared to the values reported in the literature for non-carbonated materials [59] indicating an improved inherent brittleness. The toughness index I5 of the carbonated fly ash mortars is even lower while the I₁₀ cannot be calculated due to the limited post-peak load-CMOD stage. This is an indicator of the highly brittle behavior of the carbonated fly ash-mortar specimens as a result of the high CaCO3 content (Table 3) due to the fly ash addition. The addition of biochar however greatly increases the post-crack energy absorption capacity of carbonated cementitious materials. The carbonated biochar-mortar and fly ash mortars exhibit 41% and 64% higher toughness indices I₅ and I₁₀ compared to the reference carbonated OPC material, respectively (Fig. 15). The increase in the toughness indices of the carbonated biochar enriched samples; hence their enhanced post-crack strain energy absorption capacity/strain softening behavior is

attributed to the angular and fibrillar morphology of biochar that contributes to an effective stress redistribution into the matrix and the development of more tortuous and articulated crack paths. Typical fracture surfaces of the notched cement composite samples are presented in Fig. 16. The fracture surfaces of the plain OPC mortars are smooth and sharp indicating a typical brittle fracture pattern of carbonated cementitious materials as compared to the biochar cement mixes that show a deflected crack growth pattern and much less linear crack propagation [9,60].

3.4.1. Microstructure development on carbonation

Fig. 17 (a), (b) and (c) illustrate the morphology of carbonated OPC and biochar-enriched OPC fractured mortar specimens. From Fig. 17 (a), in carbonated OPC matrix, a crystalline layer over the surface of hydrated cement particles is observed, which restricts the identification of the individual hydration products. To observe the elemental composition of the surface deposited over hydration products, elemental mapping and the EDS spectrum on the SEM images were used. According to the resulting spectrum, the layer is predominantly consisting of Ca, C, Si and O components, which indicates the formation of carbonate microcrystals in the scattered form around the hydration products.

Hexagonal and cubical-shaped crystals are presented in the SEM micrograph of the carbonated OPC-biochar sample in Fig. 17 (b). The observation suggests the precipitation of calcium carbonates together with the partially carbonated hydration products. The formation of calcium carbonate as hexagonal plate-like and cubical-shaped crystals in the carbonated cementitious matrix has also been reported in the

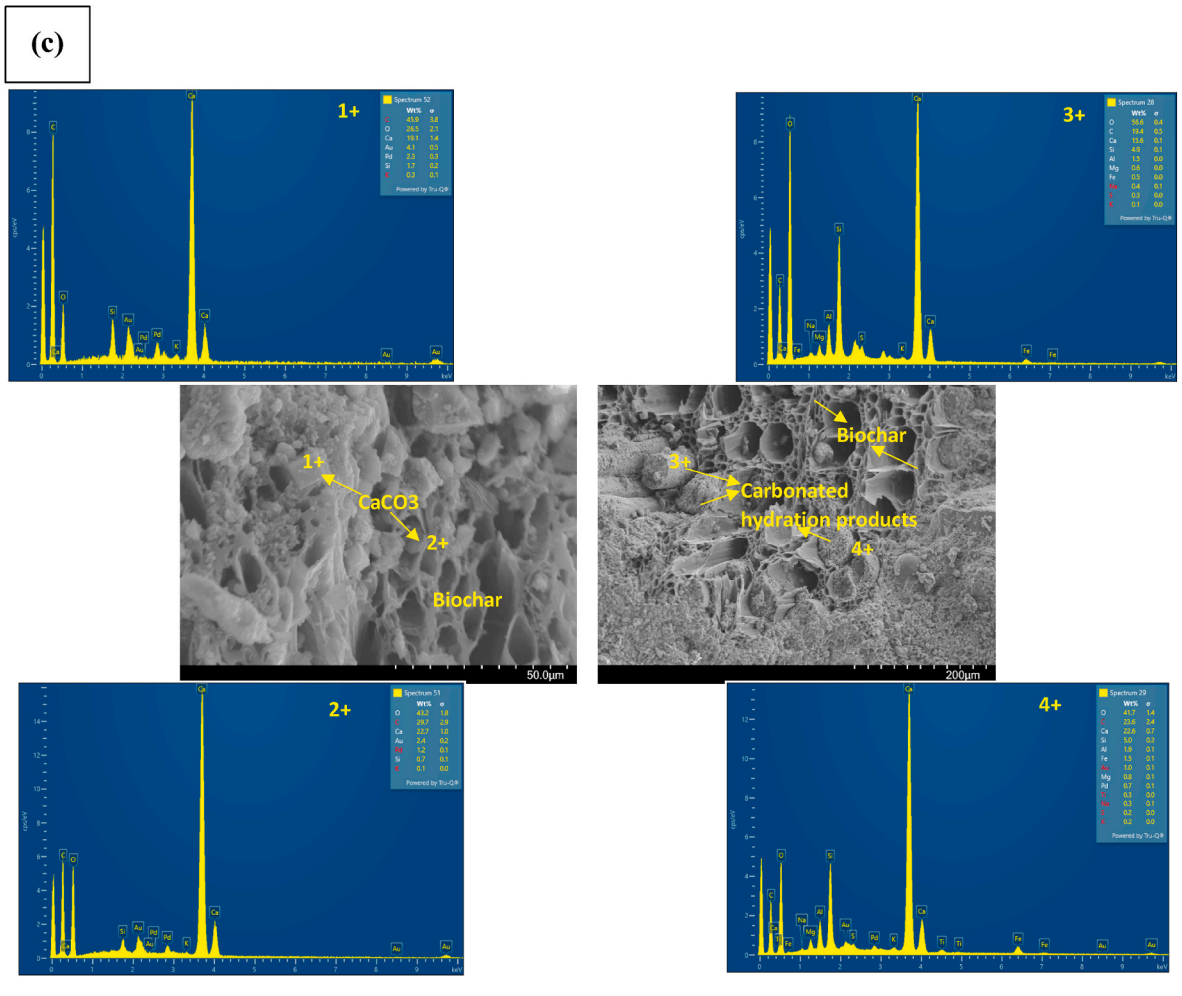


Fig. 17. (continued).

literature [61,62]. The elemental mapping of several points in the carbonated OPC-biochar sample are presented in Fig. 17 (b) and (c). The EDS spectra show that the major elements observed in the carbonated sample are Ca, O, and C indicating the formation of CaCO $_3$ crystals. It is speculated that biochar provides additional surface for CO $_2$ adsorption due to its high micro-porous surface area and structure. Upon carbonation, the dissolution of Ca $^{2+}$ ions from the hydration products and CO_3^{2-} from the adsorbed CO $_2$ leads to the in-situ precipitation of calcium carbonates onto the biochar surface. It can be seen from Table 4 and Fig. 15 that this CO $_2$ mineralization process results in a very good enhancement in the resiliency and ductility of the carbonated biochar-enriched mortars, as indicated by $\approx 10\%$ increase in flexural strength and 40–65% enhancement post-cracking energy absorption capacity.

4. Conclusions

This study investigated the viability of using biochar in combination with fly ash and/or nano silica for improving carbon capture and storage capacity, hydration, strength, and fracture properties of cementitious systems. Utilizing biochar in a cementitious system provides the opportunity to capture additional $\rm CO_2$ from the atmosphere and store it in a thermodynamically stable form of calcite within the cement matrix. The addition of 1% biochar alone increases $\rm CO_2$ uptake by 42%, however, the combination of 10% class C fly ash enhances the uptake potential to 92%, owing to the availability of additional calcium from class C fly ash, which promotes carbonate mineralization. The inclusion of biochar improved the fracture properties of carbonated fly ash-biochar

mix, as evidenced by a 20% increase in modulus of elasticity compared to reference carbonated OPC, and a 64% increase in resistance to crack propagation, as expressed by the toughness index I_{10} . The findings of SEM-EDS confirmed our hypothesis that the porous shape of biochar facilitates $\rm CO_2$ absorption and the in-situ mineralization of calcium carbonate, resulting in a denser and stronger cement matrix. From the results, we can conclude that combining mineral additives with biochar offers a feasible and sustainable prospect in offsetting the net embodied $\rm CO_2$ emissions and developing carbon-neutral concrete while providing better performance and excellent $\rm CO_2$ storage capacity compared to traditional Portland cement-based concrete.

Declaration of competing interest

The authors declare that they have no known competing financial interests or personal relationships that could have appeared to influence the work reported in this paper.

Data availability

Data will be made available on request.

Acknowledgments

The authors would like to acknowledge the financial support of the National Science Foundation-Partnerships for International Research and Education (PIRE) Research Funding Program "Advancing International Partnerships in Research for Decoupling Concrete Manufacturing

and Global Greenhouse Gas Emissions" (NSF-PIRE-2230747). Proton Power, Inc. Is kindly acknowledged for supplying biochar. The help provided by the Ph.D. student at the Center for Advanced Construction Materials of The University of Texas at Arlington, Myrsini Maglogianni, is greatly appreciated.

References

- [1] H.W. Lei, S.J. Ren, J. Julson, The effects of reaction temperature and time and particle size of corn stover on microwave pyrolysis, Energy Fuel. 23 (2009) 3254–3261.
- [2] H. Maljaee, R. Madadi, H. Paiva, L. Tarelho, V.M. Ferreira, Incorporation of biochar in cementitious materials: a roadmap of biochar selection, Construct. Build. Mater. 283 (2021), 122757.
- [3] Fawzy, et al., Industrial biochar systems for atmospheric carbon removal: a review, Environ. Chem. Lett. 19 (2021) 3023–3055.
- [4] K.G. Roberts, B.A. Gloy, S. Joseph, N.R. Scott, J. Lehmann, Life cycle assessment of biochar systems: estimating the energetic, economic, and climate change potential, Environ. Sci. Technol. 44 (2) (2009) 827–833.
- [5] M. Samoraj, M. Mironiuk, A. Witek-Krowiak, G. Izydorczyk, D. Skrzypczak, K. Mikula, S. Baśladyńska, K. Moustakas, K. Chojnacka, Biochar in environmentally friendly fertilizers - prospects of development products and technologies, Chemosphere 296 (2022), 133975.
- [6] W.C. Choi, H.D. Yun, J.Y. Lee, Mechanical properties of mortar containing biochar from pyrolysis, Journal of the Korea Institute for Structural Maintenance and Inspection 16 (2012) 67–74.
- [7] S. Gupta, H.W. Kua, S. Dai Pang, Biochar-mortar composite: manufacturing, evaluation of physical properties and economic viability, Construct. Build. Mater. 167 (2018) 874–889.
- [8] S. Gupta, H.W. Kua, H.J. Koh, Application of biochar from food and wood waste as green admixture for cement mortar, Sci. Total Environ. 619 (2018) 419–435.
- [9] S. Gupta, H.W. Kua, C. Y Low, Use of biochar as carbon sequestering additive in cement mortar, Cement Concr. Compos. 87 (2018) 110–129.
- [10] R.A. Khushnood, S. Ahmad, P. Savi, J.-M. Tulliani, M. Giorcelli, G.A. Ferro, Improvement in electromagnetic interference shielding effectiveness of cement composites using carbonaceous nano/micro inerts, Construct. Build. Mater. 85 (2015) 208–216.
- [11] R.A. Mensah, V. Shanmugam, S. Narayanan, S.M.J. Razavi, A. Ulfberg, T. Blanksvärd, F. Sayahi, P. Simonsson, B. Reinke, M. Försth, G. Sas, D. D Sas, O. Das, Biochar-added cementitious materials—a review on mechanical, thermal, and environmental properties, Sustainability 13 (2021) 9336.
- [12] S. Gupta, H.W. Kua, C. Y Low, Use of biochar as carbon sequestering additive in cement mortar. Cement Concr. Compos. 87 (2018) 110–129.
- [13] L. Wang, L. Chen, D.C.W. Tsang, H.W. Kua, J. Yang, Y.S. Ok, S. Ding, D. Hou, C. S. Poon, The roles of biochar as green admixture for sediment-based construction products, Cement Concr. Compos. 104 (2019), 103348.
- [14] S. Ahmad, R.A. Khushnood, P. Jagdale, J.M. Tulliani, G.A. Ferro, High performance self-consolidating cementitious composites by using micro carbonized bamboo particles. Mater. Des. 76 (2015) 223–229.
- [15] L. Restuccia, A. Reggio, G.A. Ferro, R. Kamranirad, Fractal analysis of crack paths into innovative carbon-based cementitious composites, Theor. Appl. Fract. Mech. 90 (2017) 133–141.
- [16] S. Ahmad, J.M. Tulliani, G.A. Ferro, R.A. Khushnood, L. Restuccia, P. Jagdale, Crack path and fracture surface modifications in cement composites, Fracture and Structural Integrity 34 (9) (2015) 524–533.
- [17] I. Cosentino, L. Restuccia, G.A. Ferro, J.M. Tulliani, Type of material, pyrolysis conditions, carbon content and size dimensions: the parameters that influence the mechanical properties of biochar cement-based composites, Theor. Appl. Fract. Mech. 103 (2019), 102261.
- [18] S. Gupta, P. Krishnan, A. Kashani, H.W. Kua, Application of biochar from coconut and wood waste to reduce shrinkage and improve physical properties of silica fume-cement mortar, Construct. Build. Mater. 262 (2020), 120688.
- [19] A. Akhtar, A.K. Sarmah, Novel biochar-concrete composites: manufacturing, characterization and evaluation of the mechanical properties, Sci. Total Environ. 616–617 (2018) 408–416.
- [20] S. Gupta, A. Kashani, A.H. Mahmood, T. Han, Carbon sequestration in cementitious composites using biochar and fly ash – effect on mechanical and durability properties, Construct. Build. Mater. 291 (2021), 123363.
- [21] A. Souto-Martinez, E.A. Delesky, K.E. Foster, W.V. Srubar III, A mathematical model for predicting the carbon sequestration potential of ordinary Portland cement (OPC) concrete, Construct. Build. Mater. 147 (2017) 417–427.
- [22] V.G. Papadakis, Effect of supplementary cementing materials on concrete resistance against carbonation and chloride ingress, Cement Concr. Res. 30 (2000) 291–299.
- [23] T. Bremner, P. Eng, Environmental aspects of concrete: problems and solutions, in: All-Russian Conference on Concrete and Reinforced Concrete, 2001.
- [24] Agnieszka Ćwik, Ignasi Casanova, Rausis Kwon, Nikolaos Koukouzas, Katarzyna Zarębska, Carbonation of high-calcium fly ashes and its potential for carbon dioxide removal in coal fired power plants, J. Clean. Prod. 202 (2018) 1026–1034.
- [25] ASTM C778 17 Standard Specification for Standard Sand.
- [26] ASTM C618-19 Standard Specification for Coal Fly Ash and Raw or Calcined Natural Pozzolan for Use in Concrete.

- [27] S. Gupta, H.W. Kua, Effect of water entrainment by pre-soaked biochar particles on strength and permeability of cement mortar, Construct. Build. Mater. 159 (2018) 107-125
- [28] ASTM C1679 Standard Practice for Measuring Hydration Kinetics of Hydraulic Cementitious Mixtures Using Isothermal Calorimetry.
- [29] ASTM C1879 Standard Test Method for Thermogravimetric Analysis of Hydraulic Cement.
- [30] X. Yang, X.Y. Wang, Hydration-strength-durability-workability of biochar-cement binary blends, J. Build. Eng. 42 (2021), 103064.
- [31] J.I. Bhatty, K.J. Reid, Use of thermal analysis in the hydration studies of a type 1 portland cement produced from mineral tailings, Thermochim. Acta 91 (1985) 95–105
- [32] H. Mehdizadeh, X. Jia, K.H. Mo, T.C. Ling, Effect of water-to-cement ratio induced hydration on the accelerated carbonation of cement pastes, Environ. Pollut. 280 (2021), 116914.
- [33] S.P. Shah, S.E. Swartz, C. Ouyang, Fracture Mechanics of Concrete: Application of Fracture Mechanics to Concrete, Rock and Other Quasi-Brittle Materials, John Wiley and Sons, New York, 1995.
- [34] E.E. Gdoutos, M.S. Konsta-Gdoutos, P.A. Danoglidis, Portland cement mortar nanocomposites at low carbon nanotube and carbon nanofiber content: a fracture mechanics experimental study, Cement Concr. Compos. (2016) 110–118.
- [35] Rilem TC 89-FMT Fracture mechanics of concrete, determination of fracture parameters (KIcs and CTODc) of plain concrete using three-point bend tests, Mater. Struct. 23 (6) (1990) 457–460.
- [36] B.I.G. Barr, M.M. Lee, E.J. de Place Hansen, D. Dupont, E. Erdem, S. Schaerlaekens, B. Schnütgen, H. Stang, L. Vandewalle, Round-robin analysis of the RILEM TC 162-TDF beam-bending test: Part 2—approximation of δ from the CMOD response, Mater. Struct. 36 (9) (2003) 621–630.
- [37] ASTM C349-18 Standard Test Method for Compressive Strength of Hydraulic-Cement Mortars (Using Portions of Prisms Broken in Flexure).
- [38] ASTM C109/C109M 21 Standard Test Method for Compressive Strength of Hydraulic Cement Mortars (Using 2-in. Or [50 Mm] Cube Specimens).
- [39] Anne-Mieke Poppe, Geert De Schutter, Cement hydration in the presence of high filler contents, Cement Concr. Res. 35 (12) (2005) 2290–2299.
- [40] R. Palla, S.R. Karade, G. Mishra, U. Sharma, L.P. Singh, High strength sustainable concrete using silica nanoparticles, Construct. Build. Mater. 138 (2017) 285–295.
- [41] S. Kang, J. Jung, J.K. Choe, Y.S. Ok, Y. Choi, Effect of biochar particle size on hydrophobic organic compound sorption kinetics: applicability of using representative size. Sci. Total Environ. 619–620 (2018) 410–418.
- [42] L. Wang, L. Chen, C.W. Tsang Daniel, B. Guo, J. Yang, Z. Shen, D. Hou, Y.S. Ok, C. S. Poon, Biochar as green additives in cement-based composites with carbon dioxide curing, J. Clean, Prod. 258 (2020), 120678.
- [43] W.C. Choi, H.D. Yun, J.Y. Lee, Mechanical properties of mortar containing bio-char from pyrolysis, Journal of the Korea Institute for Structural Maintenance and Inspection 16 (3) (2012) 67–74.
- [44] W. Liu, K. Li, S. Xu, Utilizing bamboo biochar in cement mortar as a bio-modifier to improve the compressive strength and crack-resistance fracture ability, Construct. Build. Mater. 327 (2022), 126917.
- [45] S. Praneeth, R. Guo, T. Wang, B.K. Dubey, A.K. Sarmah, Accelerated carbonation of biochar reinforced cement-fly ash composites: enhancing and sequestering CO2 in building materials, Construct. Build. Mater. 244 (2020), 118363.
- [46] P.P. Abhilash, D.K. Nayak, B. Sangoju, R. Kumar, V. Kumar, Effect of nano-silica in concrete; a review, Construct. Build. Mater. (2021), 122347.
- [47] X. Shi, Y. Yao, L. Wang, C. Zhang, I. Ahmad, A modified numerical model for predicting carbonation depth of concrete with stress damage, Construct. Build. Mater. 304 (2021), 124389.
- [48] S. Steiner, B. Lothenbach, T. Proske, A. Borgschulte, F. Winnefeld, Effect of relative humidity on the carbonation rate of portlandite, calcium silicate hydrates and ettringite, Cement Concr. Res. 135 (2020), 106116.
- [49] Caijun Shi, Z. Tu, M.Z. Guo, D. Wang, Accelerated carbonation as a fast-curing technology for concrete blocks, Sustainable and nonconventional construction materials using inorganic bonded fiber composites (2017) 313–341.
- [50] M. Fernández Bertos, S.J. Simons, C.D. Hills, P.J. Carey, A review of accelerated carbonation technology in the treatment of cement-based materials and sequestration of CO2, J. Hazard Mater. 112 (3) (2004) 193–205.
- [51] A.N. Junior, R.D. Toledo Filho, E.d.M.R. Fairbairn, J. Dweck, A study of the carbonation profile of cement pastes by thermogravimetry and its effect on the compressive strength, J. Therm. Anal. Calorim. 116 (1) (2014) 69–76.
- [52] D. Winters, K. Boakye, S. Simske, Toward carbon-neutral concrete through biochar-cement- calcium carbonate composites: a critical review, Sustainability 14 (2022) 4633.
- [53] S. von Greve-Dierfeld, B. Lothenbach, A. Vollpracht, B. Wu, B. Huet, C. Andrade, C. Medina, C. Thiel, E. Gruyaert, H. Vanoutrive, I.F. Saéz del Bosque, Understanding the carbonation of concrete with supplementary cementitious materials: a critical review by RILEM TC 281-CCC, Mater. Struct. 53 (6) (2020) 1–34
- [54] F. Kaddah, H. Ranaivomanana, O. Amiri, E. Rozière, Accelerated carbonation of recycled concrete aggregates: investigation on the microstructure and transport properties at cement paste and mortar scales, J. CO2 Util. 57 (2022), 101885.
- [55] A. Merah, B. Krobba, Effect of the carbonatation and the type of cement (CEM I, CEM II) on the ductility and the compressive strength of concrete, Construct. Build. Mater. 148 (2017) 874–886.
- [56] J. Jerga, Physico-mechanical properties of carbonated concrete, Construct. Build. Mater. 18 (9) (2004) 645–652.

- [57] H. Zhang, C. Shen, P. Xi, K. Chen, F. Zhang, S. Wang, Study on flexural properties of active magnesia carbonation concrete with fly ash content, Construct. Build. Mater. 187 (2018) 884–891.
- [58] P.A. Danoglidis, E.E. Gdoutos, M.S. Konsta-Gdoutos, Designing carbon nanotube and nanofiber-polypropylene hybrid cementitious composites with improved preand post-crack load carrying and energy absorption capacity, Eng. Fract. Mech. 262 (2022), 108253.
- [59] M. Taylor, F.D. Lydon, B.I.G. Barr, Toughness measurements on steel fiberreinforced high strength concrete, Cement Concr. Compos. (4) (1997) 329–340.
- [60] D. Suarez-Riera, L. Restuccia, G.A. Ferro, The use of Biochar to reduce the carbon footprint of cement-based materials, Procedia Struct. Integr. 26 (2020) 199–210.
- [61] Ö. Cizer, C. Rodriguez-Navarro, E. Ruiz-Agudo, et al., Phase and morphology evolution of calcium carbonate precipitated by carbonation of hydrated lime, J. Mater. Sci. 47 (2012) 6151–6165.
- [62] H. Choi, H. Choi, M. Inoue, R. Sengoku, Control of the polymorphism of calcium carbonate produced by self-healing in the cracked part of cementitious materials, Appl. Sci. 7 (2017) 546.